CHAPTER 6

Numerical study on the spray and thermal characteristics of cryospray process

The aim of the study is the real time estimation of freezing front and lethal front in the lesion so that spraying distance and spray duration can be optimised for different lesion dimensions. The cryospray process involves complex physical processes like interaction of liquid nitrogen spray with surrounding through convection and evaporation, impingement of liquid nitrogen on the skin, and phase change of tissue involving latent heat release. Earlier researchers have applied series of assumptions to simplify the complex phenomena of cryospray (for necrosis) while modeling it. Predominantly only heat interactions below the gel surface is simulated. Furthermore, they have used several assumptions like application of time dependent temperature boundary condition on the gel surface [96, 97] or variation in the convective heat transfer coefficient on the gel surface [160]. In the present case, each and every aspect of cutaneous cryospray from nozzle exit to tissue surface is acknowledged whereas the sensible and latent heat interaction beneath the tissue surface is also modeled.

6.1 Mathematical model and numerical approach

In-vitro experiment of cryospray is shown in fig. 6.1. The details of cryospray experiments can be found elsewhere [156]. For simplification purpose, flow inside the cryogun and nozzle is not simulated in the present case. The domain of computational investigation

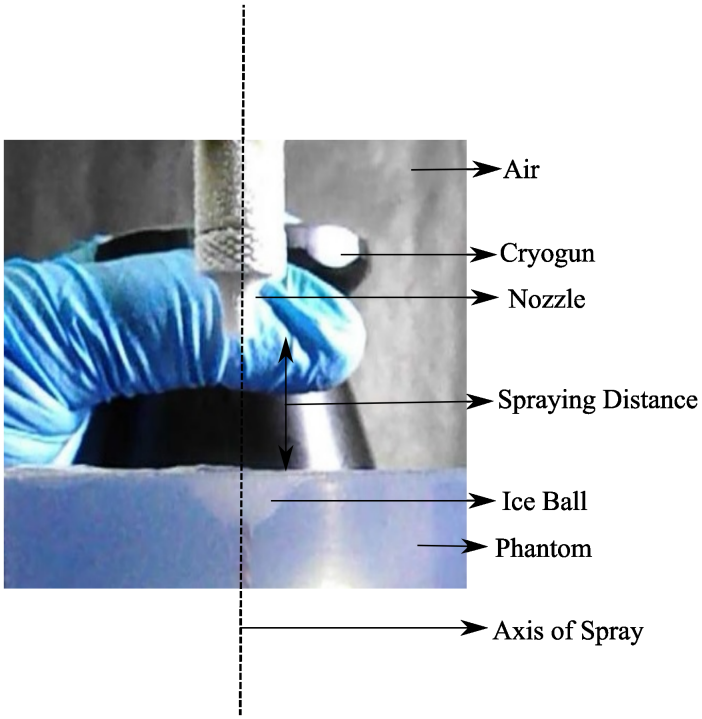

Figure 6.1: Actual Cryospray Process

is based on the interaction of cryogen with the surrounding and tissue phantom. Since the problem is symmetric, an axisymmetric flow is simulated because it reduces the computational cost and simulation time (refer fig. 6.2) [85, 124]. Two blocks are made in the computational domain. Top one represents the air region whereas the lower one represents the tissue phantom region. The atomised droplets of cryogen are discharged from the inlet (nozzle exit) in the model parallel to the axis of spray.

6.1.1 Governing equations

Interaction of cryogen with the surrounding is solved by Eulerian-Lagrangian approach. Air is considered as continuous phase whereas the droplets of cryogen are considered as dispersed phase. Eulerian framework is utilised to describe turbulent flow heat transfer of continuous phase while Lagrangian framework is used to describe the evaporation of dispersed phase.

6.1.1.1 Continuous phase (air)

The Reynolds averaged Navier-Stokes (RANS) equations along with realizable k-ε turbulent model are solved to study the turbulent flow field of continuous phase. It has been

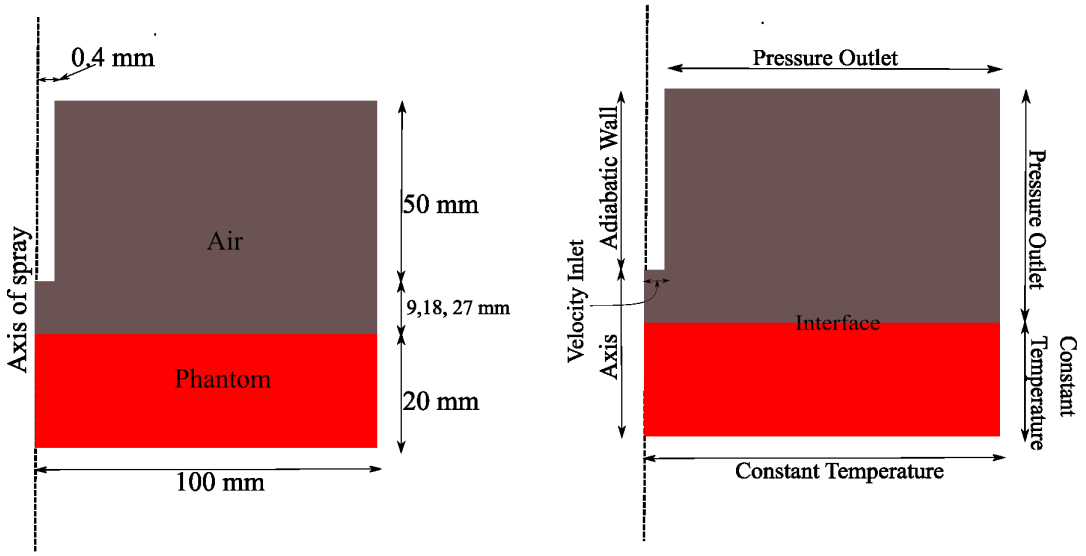

(a) Dimensions of Domain (b) Boundary Conditions

Figure 6.2: Computational Doamin

observed that realizable k-ε turbulent model provides improved results than standard k-ε turbulent model [11, 124]. Montarzi et al. [113] have employed RANS equations in combination with realizable k-ε turbulent model to solve conservation equations of mass, momentum and energy for three dimensional steady flow. They have compared several turbulence models for the continuous phase and concluded that realizable k-ε turbulent model is suitable for studying the influence of evaporating cooling in water spraying systems [113]. However, Feng et al. [56] have used standard k-ε turbulent model in the study of atomized droplets evaporation in flue gas flow. Another reason for the selection of realizable k-ε turbulent model is its ability to predict the spreading rate for axisymmetric jets as well as the planner jets [150]. Other traditional k-ε turbulent models provide poor result in case of axisymmetric jet. In order to consider the influence of droplet evaporation on continuous phase, source terms are introduced in the governing equations of the continuous phase.

$$\frac{\partial \rho_g}{\partial t} + \nabla.(\rho_g u_g) = S_p \tag{6.1}$$

$$\frac{D(\rho_g u_g)}{Dt} = -\nabla p + \mu_g \nabla^2 u_g + \rho_g g + S_f \tag{6.2}$$

$$\frac{\partial(p_g Y)}{\partial t} + \nabla.(\rho_g Y u_g) = div(\rho_g D_Y grad Y) + S_Y \tag{6.3}$$

$$\frac{\partial(\rho_g h_g)}{\partial t} + \nabla.(\rho_g h_g u_g) = div(\lambda_g grad T_g) + S_h \tag{6.4}$$

The corresponding source term of each equation account for the influence of droplets on continuous phase. They are calculated through lagrangian approach and further incorporated into the continuous phase.

6.1.1.2 Discrete phase (liquid nitrogen droplets)

Flashing occurs in liquid nitrogen as it ejects from the commercial cryospray nozzle of diameter 0.8 mm. Flash evaporation occurs when the saturated liquid undergoes reduction in pressure below its saturation pressure [178]. Cryogun stores liquid nitrogen above atmospheric pressure, as the valve is opened the liquid nitrogen enters into the metastable state due to the rapid depressurisation [14]. It causes nucleation of bubbles inside (cannula and nozzle geometry) the cryogun and finely atomised spray is obtained due to the dynamic expansion of cryogen bubbles that shatters the streams of liquid nitrogen [175]. A continuous heat and mass transfer takes place on the interface of droplet and air during its flight from nozzle exit to gel surface. The droplets will continuously evaporate during their interaction with the surrounding and eventually vanish depending on their size. It occurs due to temperature difference between the liquid nitrogen (-196 ^{0}C) and air (27 ^{0}C). The rate of energy absorbed by each droplet, considering the single droplet evaporation mechanism with an assumption that droplets have no internal thermal resistance, is described in eq. 6.5. The sensible heat change in the droplet can be equated to the latent and convective heat transfer interaction between the continuous phase and the dispersed phase.

$$m_d c_p \frac{dT_d}{dt} = h_c A_d (T_g - T_d) - \frac{dm_d}{dt} L_h \tag{6.5}$$

The convective heat transfer coefficient between air and cryogen is estimated using Ranz-Marshall empirical equation (refer eq. 6.6). It is used for the prediction of Nusselt and Sherwood numbers which describe the heat and mass transfer between the droplet surface and the moving gas; details can be found elsewhere [49, 56, 175].

$$Nu = \frac{h_c d_d}{\lambda_g} = \frac{ln(1+B_T)}{B_T}(2+0.6Re_d^{0.5}Pr^{0.33}) \tag{6.6}$$

Newtons second law is utilised to calculate the trajectory of particles using lagrangian method and including the influence of relevant forces from the continuous phase. Spherical droplets of uniform density and temperature are assumed to be entering in the computational domain. Only drag force and gravity force are considered in predicting the motion of droplets (refer eq. 6.7). Other forces like lift, buoyancy and virtual mass force are neglected because the density of cryogen is greater than the density of air [111].

$$\frac{d\overrightarrow{u_d}}{dt} = \overrightarrow{g} + \frac{\Sigma\overrightarrow{F_d}}{m_d} \tag{6.7}$$

6.1.1.3 Phase change in gel phantom

It has been assumed that the conduction is the only mode of heat transfer in gel phantom. Enthalpy-porosity approach is used to model solidification in gel phantom region [172]. In this technique liquid fraction, which represents the volume of liquid in each cell, is introduced in each cell. Enthalpy balance is used to compute the liquid fraction in each cell. For non-eutectic solidification, mushy zone is introduced (region in which liquid fraction ranges between 0 and 1). It is treated as pseudo porous medium in which porosity decreases from 1 to 0 as the material solidifies. The porosity of the material becomes 0 when it fully solidifies and the velocities drops to zero. Therefore, the energy equation is solved as

$$\frac{\partial(\rho H)}{\partial t} = \nabla.(k\nabla T) \tag{6.8}$$

where, enthalpy (H) is calculated as the sum of latent heat (h_l) and sensible heat (h_c)

$$H = h_c + h_l$$

$$h_c = h_{ref} + \int_{T_{ref}}^{T} c_p dT$$

$$h_l = \beta L$$

β represents the liquid fraction, $\beta = 0$ if T < $T_{solidus}$

$\beta = 1$ if T > $T_{liquidus}$

β = (T - $T_{solidus}$) / ($T_{liquidus}$ - $T_{solidus}$), when $T_{solidus}$ < T < $T_{liquidus}$

6.1.2 Boundary condition and operating parameters

The mass flow rate of cryogun is measured experimentally to validate the numerical model with the experimental results [83, 123]. Cryogun of 500 ml is filled with the liquid nitrogen upto a specified mark. Hold time of 10 s is provided for pressure build up. Meanwhile, single hole nozzle of 0.8 mm is mounted on the exit and placed on the weighing balance. The 12 different spray durations viz; 5 s, 10 s, 15 s, - - - -, 60 s are selected and the readings of weighing balance is recorded to approximate instantaneous mass flow rate. Each experiment is conduced thrice to ensure repeatability in results. Uncertainty of ±0.1 grams is observed in the measurements. The least count of weighing balance was 0.1 grams. Similar approach to calculate mass flow rate of cryogen are used by Vu et al. [173] and Xue et al. [179]. The overall mass flow is found to be 0.00016 kg/s after 1 minute of spray whereas the instantaneous mass with respect to time step is shown in fig. 6.3. Mass flow rate is less during initial phases of spray because liquid cryogen undergoes the flashing process inside the cannula of cryogen and the nozzle geometry. When the valve is opened, single phase flow of cryogen changes into two-phase flow in the cannula due to depressurisation and temperature difference between the cryogen and walls of the cannula. It further amplifies as it enters in the nozzle geometry due to larger area and higher temperature difference. Hence atomisation occurs in the bubbles of liquid cryogen and they turn into discrete droplets at the nozzle exit [175]. As the time proceeds, the temperature difference reduces and mass flow rate increases. The size distribution of particles is assumed to follow the Rosin-Rammler model. The minimum diameter of particle is taken as 20 μm whereas the maximum diameter of particle is taken as 100 μm with mean diameter of 80

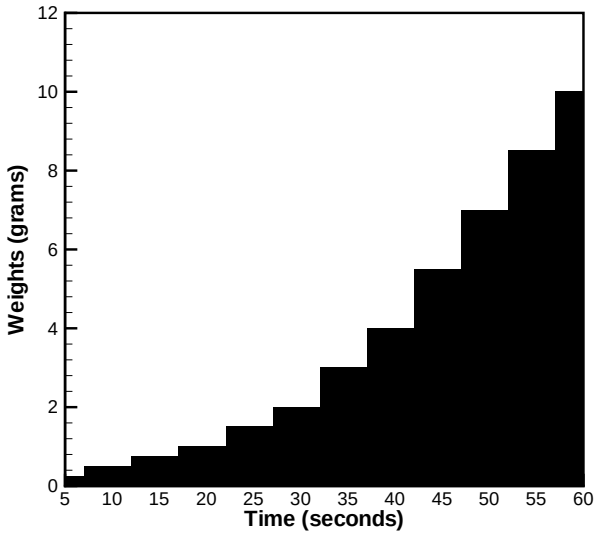

Figure 6.3: Mass flow rate

μm. The spread parameter which signifies the distribution width of particles is selected to be 3.5. Surface injection from inlet (refer fig. 6.2b) is chosen to introduce cryogen droplet in the computational domain.

Zhang et al. [186] have studied the role of operating pressure on the spray cone formation. They concluded that for lower operating pressure (< 100 kPa) the spray remains concentrated around the axis of spray. Experimental investigation conducted by Aguilar et al. [3, 4] on cryogen also established that cryogens (r134a) does not spread more in the radial direction at lower pressure (660 kPa). However, it is worth mentioning that fluids used in the former studies [3, 4, 186] are different from the fluids used in the present study. Hence, the results cannot be replicated directly in the present case. But considering experimental observations and the operating pressure (i.e., 35 kPa), it is observed that the jet remains in the closed vicinity of spray axis. Hence, surface injection is used to introduce liquid nitrogen in the computational domain. Moreover, the nozzle used in the study is solid cone type nozzle, unlike the long nozzle considered by Augilar et al. [3, 4] which allows more heat transfer. Initially air is at 27 ^{0}C whereas liquid nitrogen is at -196 ^{0}C. The various components of air (xO2 = 0.23, xH2O = 0.1 and xN2 = 0.76) are included in the domain. The model is axisymmetric so gravitational acceleration is set at 9.81 m/s^2 in the positive x-direction. Escape boundary conditions are set for the discrete phase particles at inlet and outlet which means droplets will leave the domain in their actual condition as they reach the boundary. Reflect boundary condition is set for droplets at the interface to track the rebound of droplets, as they hit the interface. It is included to acknowledge the

splashing of cryogen droplet that might occur at smaller spraying distance.

The dimension of inlet is taken as 0.4 mm to replicate the radius of commercial cryospray nozzle. The wall above the inlet and parallel to spray axis is set as adiabatic wall whereas pressure outlet boundary conditions are set at top and right walls of air domain. Phantom walls are kept at constant temperature (i.e., 27 ^{0}C). Since the maximum temperature difference in the computational domain is less than 400 K so the effect of radiation is neglected in the present case [49].

Axisymmetric domain used in the study is shown in fig. 6.2. The depth of phantom domain is taken as 20 mm whereas its length is taken as 100 mm. The spraying distance, i.e. the distance between the inlet (nozzle exit) and phantom surface is varied and taken as 9 mm, 18 mm and 27 mm respectively. The inlet boundary condition for air is set as velocity inlet; a uniform and steady velocity is assumed for air. The velocity is considered to be equivalent to stagnation pressure of the cryogun [113, 191]. Calay and Holdo. [29] have considered several methods to estimate the exit velocity viz: assuming isentropic chocked flow at the nozzle exit, maximum kinetic energy that can be obtained during liquid cooling or expansion and Bernoulli's theorem. They concluded that velocity estimated through pressure stagnation method can closely approximate the experimental result. The stagnation pressure was measured experimentally by Vu et al. [173] to estimate the exit velocity of cryogen. They have also acknowledged the different exit velocities for the continuous and discrete phases. However, they further concluded that both the phases follow similar velocity profile (same as the droplet velocity) after some distance from the nozzle exit. Hence, similar approach is applied in the present case, i.e. same velocity for the discrete and continuous phases. The average pressure at which cryogun operates is assumed to be 35 kPa, after considering the losses occurring inside it, the velocity of continuous phase and discrete phase is taken as 9 m/s in present case.

The thermo-physical properties of the tissue are function of temperature, because it is considered as nonideal substance. The phase change of tissue takes place over a temperature range depending upon its orientation [94]. Hence, liquidus and solidus temperature of tissue are set at 0 ^{0}C and -1 ^{0}C respectively with a pure solvent melting heat of 3.03x10^5 J/kg to model the phase change process. Temperature dependent specific heat and thermal conductivity are also considered for tissue [148]. Conduction is considered as the only mode of heat transfer inside the tissue because the effect of metabolic heat generation and blood perfusion are less dominant in cutaneous cryospray [157].

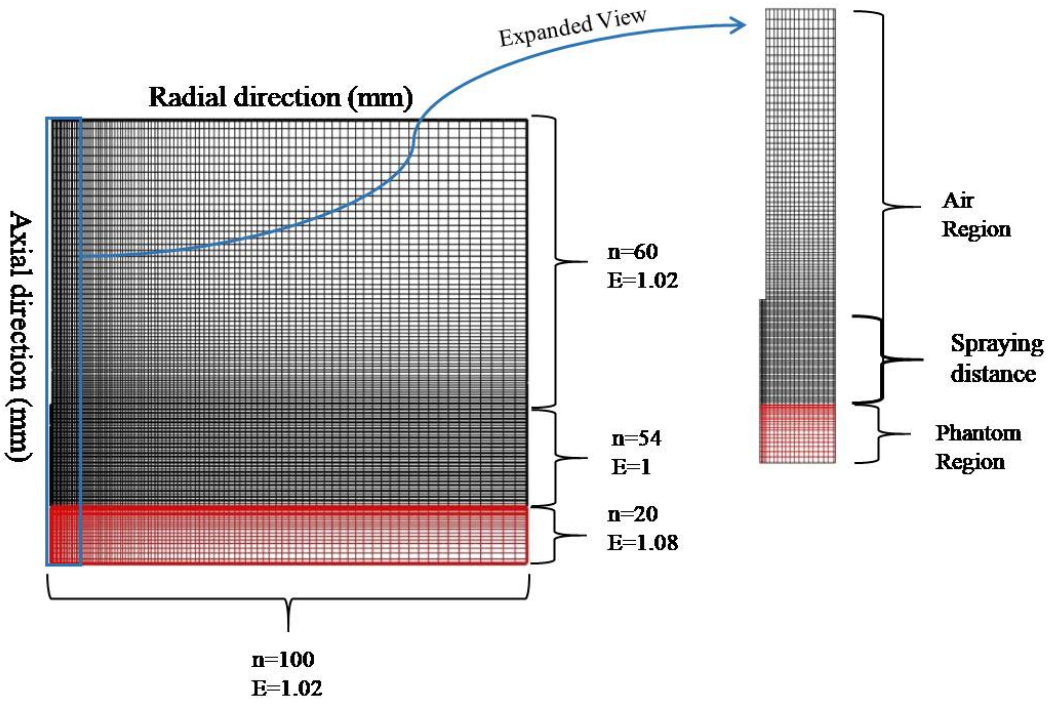

Figure 6.4: Grid distribution for computational domain

6.1.3 Numerical approach and grid distribution

Structured grid is selected to carry out the computational work while coupling the pressure and velocity with SIMPLE (Semi Implicit Pressure Linked Equation) algorithm. The convective and diffusive terms are discretised using power law and second order central difference scheme respectively. First order implicit scheme is used for the transient formulations. The normalized residual for continuity equation is set as 10^{-5} whereas for other equations it is kept at 10^{-4}. A comparative study is dedicated to analyse the influence of residuals on the solution. it has been observed that further increase in residuals does not affect the solution. A typical grid distribution for a spraying distance of z = 18 mm is shown in fig. 6.4 along with their expansion ration (E) and number of division (n). Red color represents the tissue section and black color represents the air section. Dense grids with uniform distribution are used in the spray region whereas comparatively coarse grids (than spray region) with non-uniform distribution are used in the tissue section and air section (above inlet). An enlarged section of mesh near the axis of spray is also shown in fig. 6.4 along with their dimension. For the other two cases (i.e., spraying distances z = 9 mm and z = 27 mm), only mesh in the spraying distance section is changed while keeping the same expansion ratio. The spraying distance is the distance between the nozzle exit

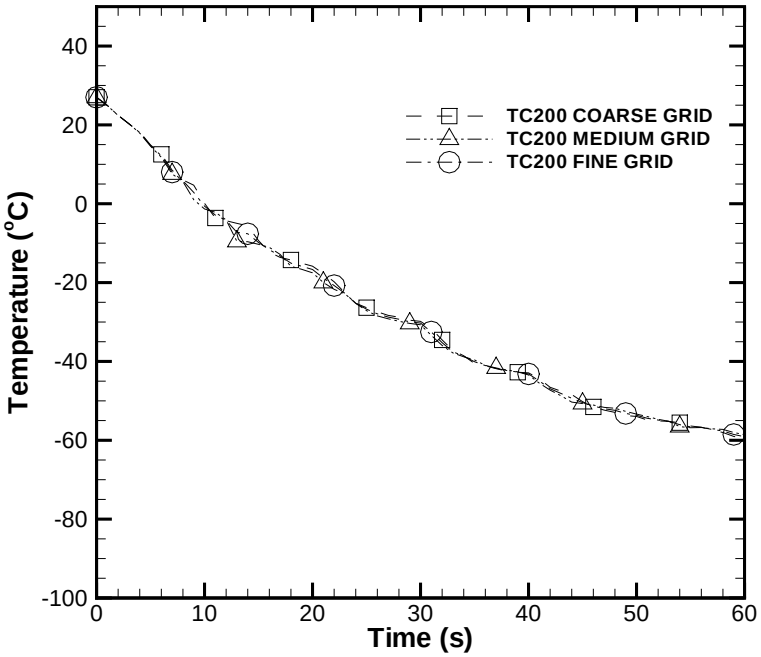

Figure 6.5: Grid indenpence test

and the tissue surface. The number of division (n) for z= 9 mm and z= 27 mm is taken as 27 and 81 respectively.

The time step is taken as 0.0005 s and a maximum of 200 iterations are provided per time step to obtain converged solution at each time interval. During each time step, 20 parcels are introduced in the computational domain.

6.1.4 Grid independence and time independence

Three different grid densities of 90 x 94 (coarse grid), 107 x 104 (medium grid), 124 x 124 (fine grid) are selected to carry out grid independence test for spraying distance z = 9 mm. The initial temperature and other input parameters are kept same for all the three cases. Results are plotted at an axial location of 2 mm below the center point of the spray. The fig. 6.5 manifests that the results are independent of grid density. Hence, grid density of 107 x 104 is selected for further study.

The time step is varied as $5x10^{-3}$, $5x10^{-4}$ and $5x10^{-5}$ to check for the time dependent study while keeping the maximum time step per iteration constant. The temperature distribution with respect to time does not show any significant change with change in the size of time step. Thus, time step size of $5x10^{-4}$ is selected for the further study.

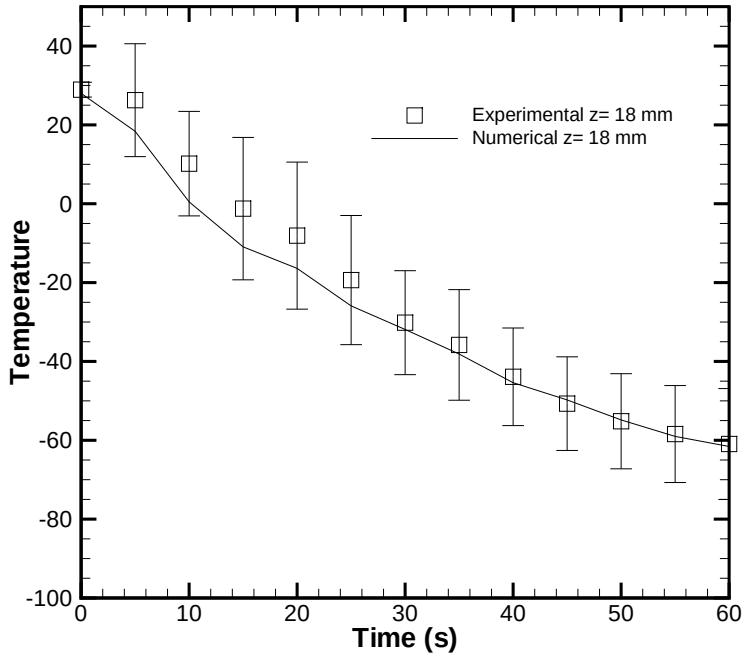

Figure 6.6: Code Validation

6.1.5 Code validation

The result obtained during the experiments conducted in our previous study with single hole nozzle is used for the code validation. A spraying distance (z) of 18 mm is selected for the code validation [156]. The transient temperature response of the thermocouple mounted at an axial depth of 2 mm from the gel surface is compared with the numerical result (refer fig. 6.6). A good agreement between the numerical and experimental results is obtained. The maximum difference in temperature between the experimental and numerical values is found to be 9 ^{0}C. It falls within the uncertainty range of experiments ($\pm$15 ^{0}C), hence it can be accepted. Moreover, it is observed during the initial phases of spray, when the mass flow rate fluctuates due to flashing inside the cryogun. Chua et al. [37] validated a numerical model of cryosurgery by comparing it with in-vitro experimental data. They have observed the similar observation, i.e. the maximum deviation between numerical and experimental results during initial phases of cryosurgery.

The numerical results are further verified with the experimental result for the ice ball propagation along and across the gel surface. The size of axial and radial ice balls obtained from different approaches is compared after 60 s of spray. The radial ice ball is 9 % larger in numerical case as compared to the experimental case. Whereas, the axial ice ball is 4 %

larger in numerical case as compared to the experimental case.

6.2 Results and discussion

The study aims at the development of numerical model that acknowledges all the parameters involved in the cryospray process; specially the rate of heat and mass transfer of cryogen with the surrounding and the tissue. It will help in the estimation of necrotic zone. Two ways coupling is adopted to examine the influence of discrete phase on the continuous phase above the gel surface whereas sensible and latent heat interactions are monitored beneath the gel surface; sensible and latent heat interactions beneath the gel surface are the consequence of heat and mass transfer occurring between the liquid nitrogen droplets and the surrounding. Influence of spraying distance on necrotic zone is also studied to ascertain the most optimised spraying distance on the basis of lesion dimension.

6.2.1 Temperature variation

The comparison of spray images (actual and numerical) representing the temperature variation in the spray domain for various spraying distances after 60 s of spray is shown in fig. 6.7, fig. 6.8 and fig. 6.9. The contours are drawn in such a way that 0 mm on abscissa represents the start of tissue domain (interface). It can be seen through the images that the cooling zone is concentrated around the spray axis for the smallest spraying distance (i.e., z = 9 mm) whereas it is less concentrated around the spray axis for the larger spraying distances (z = 18 mm and z = 27 mm). Smaller spraying distance causes less reduction in velocity and droplet diameter along spray axis thus larger droplets strike the tissue surface. It results in more evaporation of cryogen from the tissue surface around the spray axis compared to that in the peripheral region. In the case of larger spraying distance, more dispersion of cryogen droplets in the radial direction is observed during their flight due to larger interaction with the continuous phase (in terms of time). It causes a larger

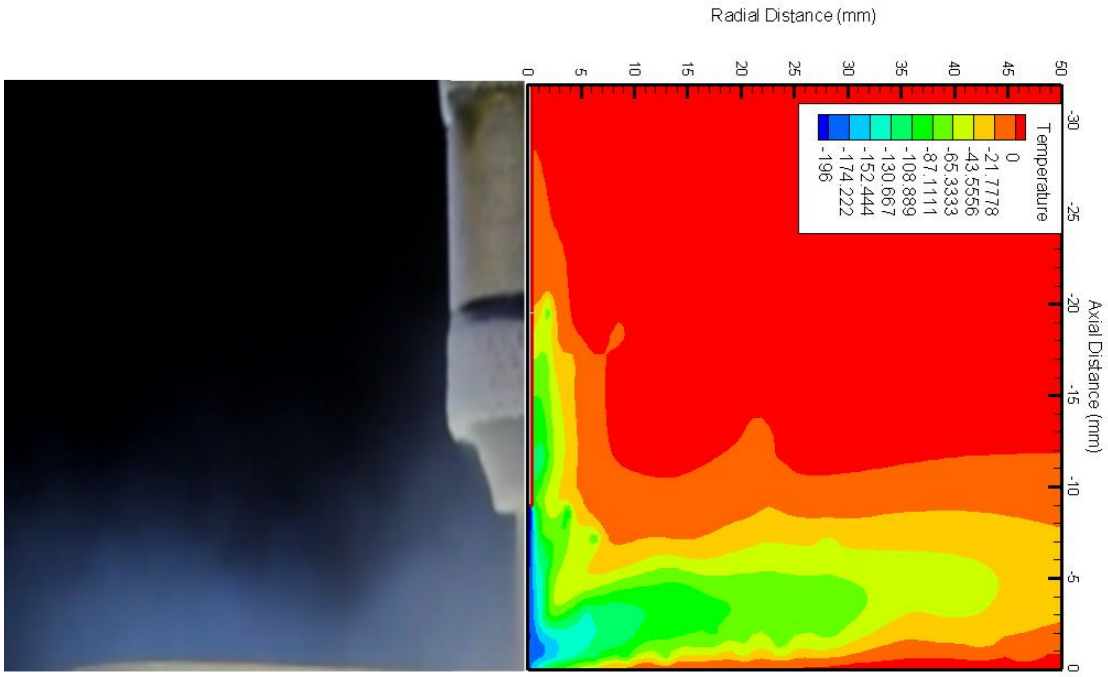

Figure 6.7: Comparison of spray image with the temperature contour of spray domain for z = 9 mm after 60 s

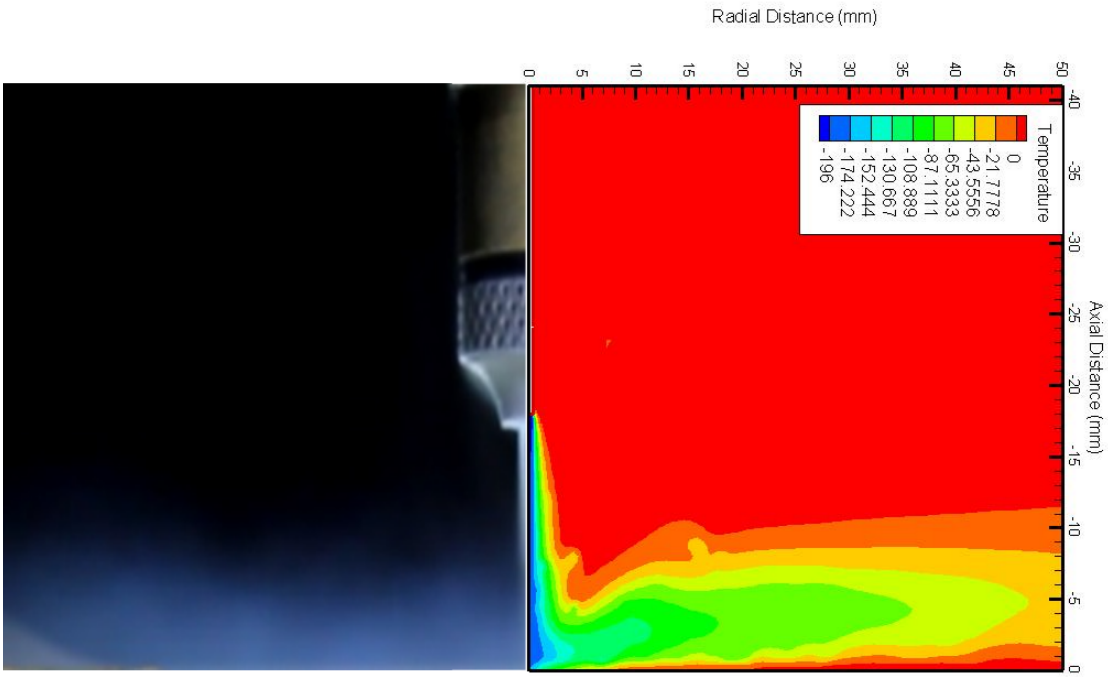

Figure 6.8: Comparison of spray image with the temperature contour of spray domain for z = 18 mm after 60 s

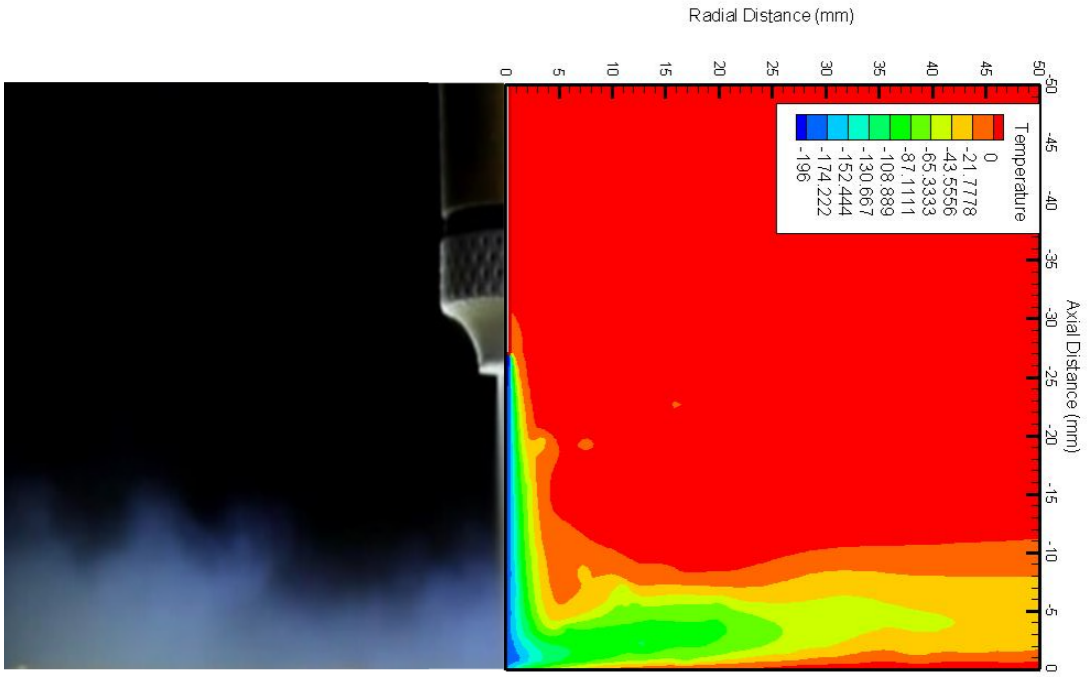

Figure 6.9: Comparison of spray image with the temperature contour of spray domain for z = 27 mm after 60 s

reduction in droplet diameter and velocity before striking the tissue surface hence less cooling is observed along spray axis (refer fig. 6.10). The dispersion of flashing R404A and R134a spray with respect to spraying distance is studied experimentally by Zhou et al.[192] and Zhifu et al.[190] respectively. They have concluded that the dilution of cryogen with ambient air increases with the increase in spraying distance leading to radial dispersion of spray. It should be noted that they have studied the spray characteristics without impingement whereas in the present case, spray impinges on the tissue. Hence, a thick layer of vapors of the cryogen can been seen in the spray images.

It can also be observed from the fig. 6.10 that there is a sudden drop in the temperature before the interface of tissue and spray. The disintegration of cryogen jet and impingement of cryogen droplets on the tissue surface are responsible factors for such variation in spray with surrounding. For the smaller spraying distance, cryogen jet remains intact and impinges on the tissue surface [193] with a greater magnitude of velocity. It causes the cryogen droplets to rebound back; hence, more fumes of cryogen approaching towards nozzle can be seen in the vicinity of spray for smaller spraying distance (refer fig. 6.7). However, for a larger spraying distance, the cryogen jet disintegrates into smaller droplets causing reduction in the associated mass of droplets. Thus, the rebound of cryo-

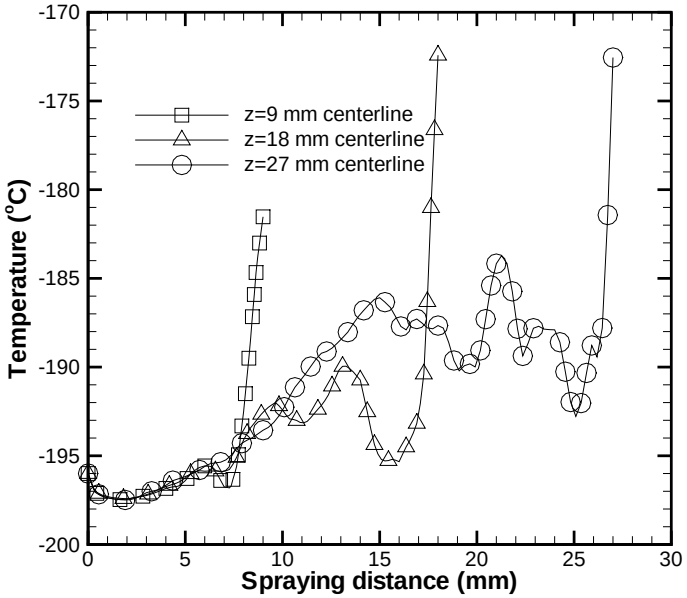

Figure 6.10: Centreline temperature distribution in the spray domain after 60 s of spray

gen droplets are not observed for z = 18 mm and z = 27 mm and a uniform layer of cryogen fumes is obtained for these spraying distance.

For z = 18 mm and z = 27 mm the sudden drop in temperature before reaching the interface is more than z = 9 mm. It is due to disintegration of the jet for the larger spraying distance which causes accumulation of smaller droplets on the interface. The lower thermal conductivity of skin causes the built up of cryogen film on the surface because of the insufficient flushing velocity and reduced evaporation rate. It serves as a barrier to heat transfer between the impinging droplets and the skin. The cryogen film is composed of residing and impinging droplets of cryogen. The dimension of cryogen film depends on various factors such as temperature gradient between cryogen and tissue, nozzle diameter, operating pressure, spraying distance and droplet diameter [122, 123, 176]. Hence, the temperature drop just above the interface is due to the formation of cryogen film. The other two valleys in the centreline of the temperature curve for z = 18 mm and z = 27 mm mark the initiation of jet disintegration which leads to reduction in temperature due to rapid evaporation. It can be seen in the images that the jet disintegration occurs approximately 8 mm and 12 mm above the interface for z = 18 mm and z = 27 mm respectively. For z = 9 mm, the sudden temperature drop along the centreline is negligible confirming the intact jet and very thin cryogen film formation due to greater flushing velocity. For all the three cases, a slight decrease in temperature is obtained near the nozzle exit.

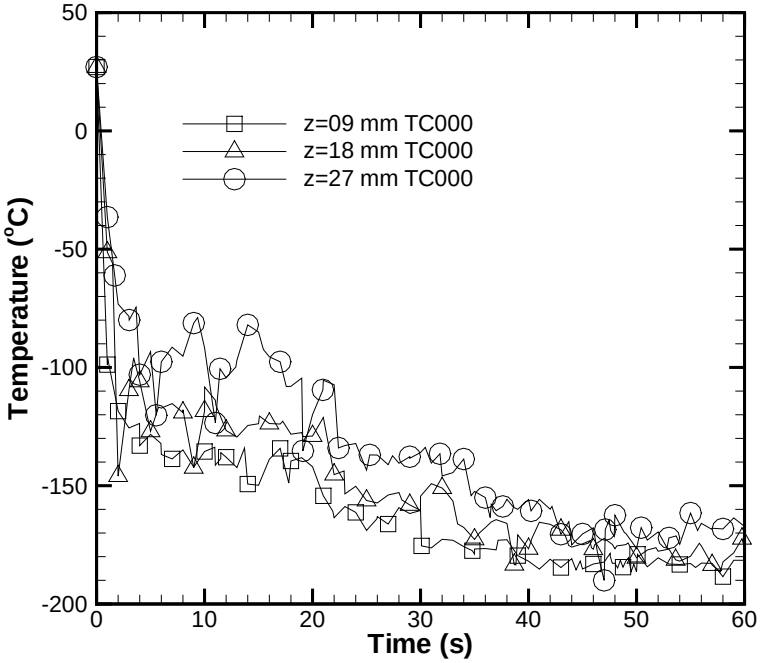

Figure 6.11: Transient temperature of a point on the tissue surface at a distance of 0 mm from the centre of spray (TC000 location)

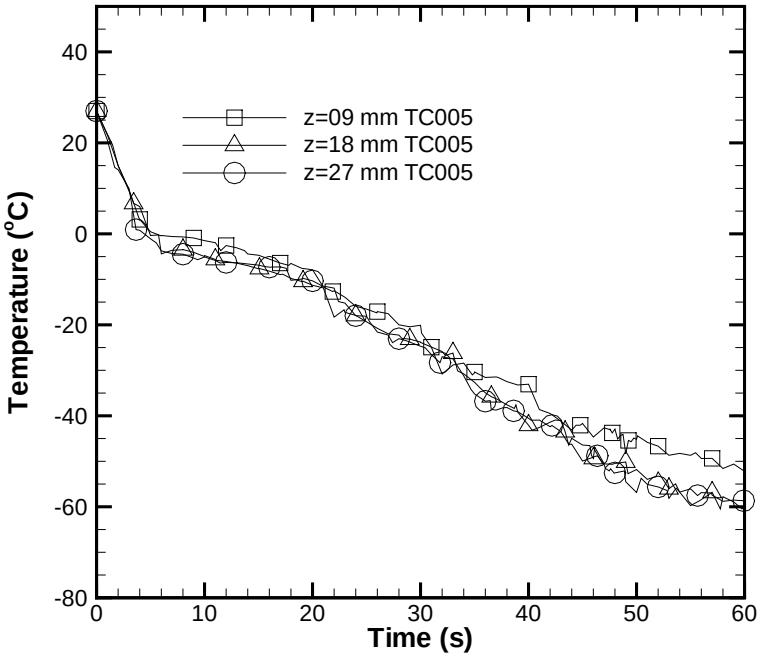

Figure 6.12: Transient temperature of a point on the tissue surface at a distance of 5 mm from the centre of spray (TC005 location)

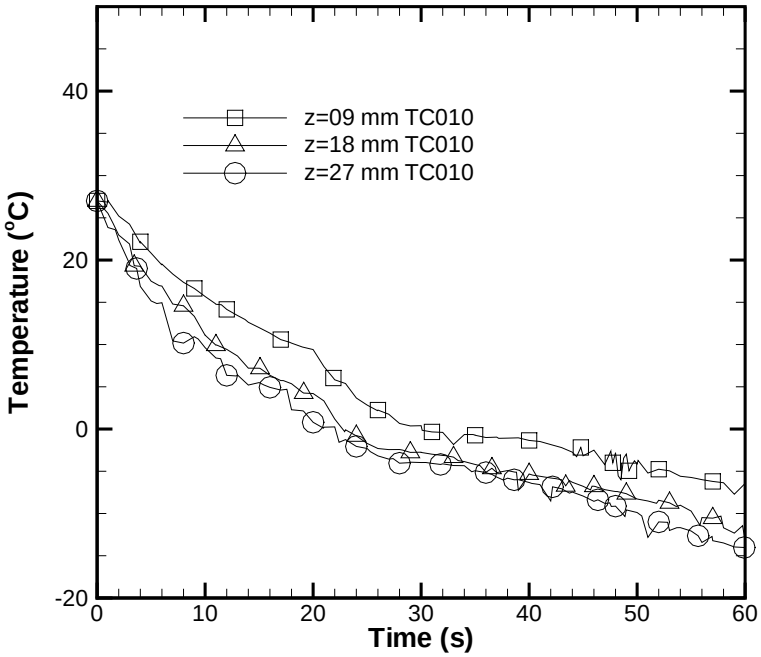

Figure 6.13: Transient temperature of a point on the tissue surface at a distance of 10 mm from the centre of spray (TC010 location)

Since larger spraying distance causes greater dispersion of cryogen in the radial direction, so heat transfer increases along the interface for larger spraying distance as shown in fig. 6.11, fig. 6.12 and fig. 6.13. For the location TC000 (which means point at the centre of spray on tissue surface), z = 9 mm is providing the lowest temperature among the three spraying distances selected for the study. However, at the location TC005 (point at a distance of 5 mm from the centre of spray on tissue surface), a large drop in temperature is noticed for the spraying distances z = 18mm and 27 mm as compared to the spraying distance z = 9 mm. It clearly demonstrates that with increase in the spraying distance cooling zone increases in the radial direction. Similar trend is observed for TC010 location (point at a distance of 10 mm from the centre of spray on tissue surface) with z = 27 mm providing the highest temperature drop due to the aforementioned reason.

6.2.2 Lethal front propagation

Lethal temperature can be defined as a temperature below which the necrosis is guaranteed. The accepted range of lethal temperature varies between -20 ^{0}C to -40 ^{0}C depending on the location of the lesion. In the present case, the lethal temperature is considered as

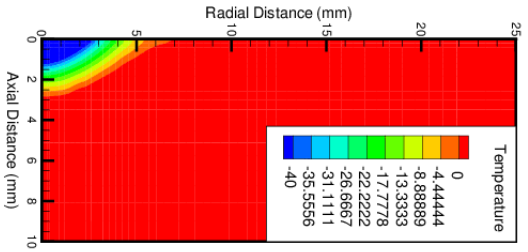

(a) For z = 9 mm

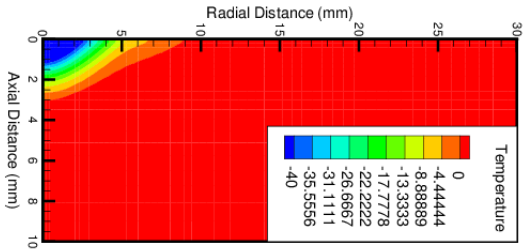

(b) For z = 18 mm

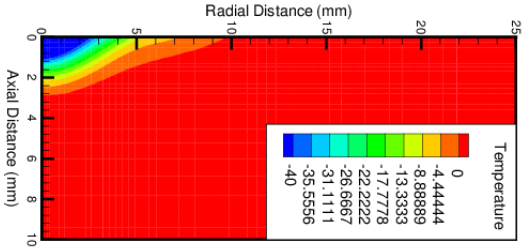

(c) For z = 27 mm

Figure 6.14: Lethal front after 20 s

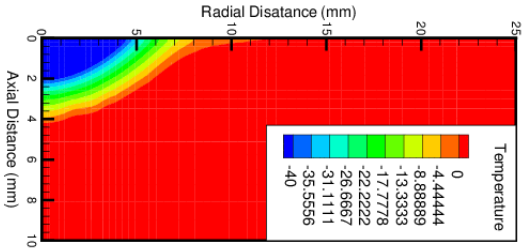

(a) For z = 9 mm

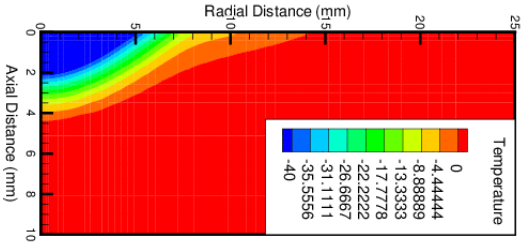

(b) For z = 18 mm

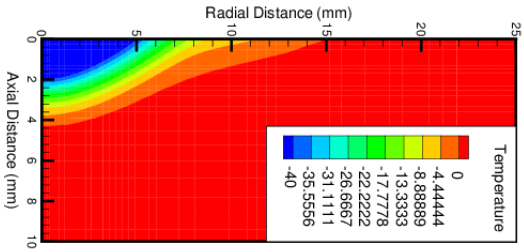

(c) For z = 27 mm

Figure 6.15: Lethal front after 40 s

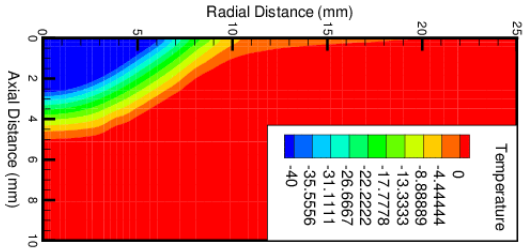

(a) For z = 9 mm

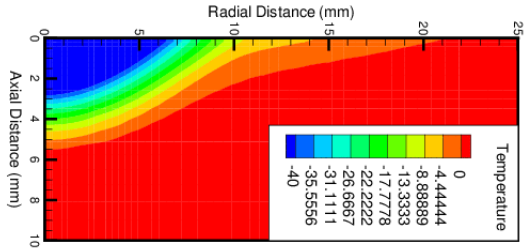

(b) For z = 18 mm

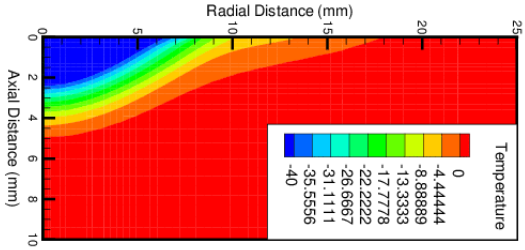

(c) For z = 27 mm

Figure 6.16: Lethal front after 60 s

-40 ^{0}C. The temperature contours of lethal fronts are shown in fig. 6.14, fig. 6.15 and fig. 6.16 after 20 s, 40 s and 60 s of spray respectively. The depth of lethal front in the axial direction is largest for z = 18 mm and smallest for z = 27 mm; for z = 18 mm it is 16.6 % larger than that for z = 27 mm. The lethal front of z = 9 mm is 12.5 % larger than the lethal front of z = 27 mm after 60 s of spray in axial direction. The spread of lethal front in the radial direction for z = 27 mm is 5 % larger than the lethal front for z = 9 mm after 60 s of spray. It means that energy transfer increases in the radial direction and reduces in the axial direction with increase in the spraying distance.

It can be observed that halo diameter increases with increase in the spraying distance; halo diameter is the difference between the radius of freezing front and lethal front of the spray. In order to achieve complete necrosis of the lesion, it should be frozen below the lethal temperature beyond its boundary [170]. A larger halo diameter signifies surplus freezing which is not required as it causes discomfort to the patient [106]. The halo diameter is largest (nearly 3.1 mm) for z = 18 mm and smallest (nearly 2.3 mm) for z = 9 mm in the axial direction after 60 s of spray. Further, in the radial direction, z = 18 mm provides largest halo diameter of 14.5 mm followed by z = 9 mm with 13.8 mm. The temperature contours provide the broader understanding in terms of halo diameter propagation in the tissue domain with respect to time. The lethal front takes a shape of ellipse in all the three cases of spraying distance under consideration. But, the regions where temperature

ranges between -40 ^{0}C to 0 ^{0}C (halo diameter) are different for different spraying distances. The halo diameter is thick along the periphery of lethal front for z = 27 mm as compared to z = 9 mm. It means that the cooling zone is less diffused in tissue domain for the smaller spraying distance compared to the larger spraying distance, where more diffusion is observed. The temperature distribution across the line drawn at an angle of 30 ^{0} (line 1) and 60 ^{0} (line 2) from the spray axis after 60 s of spray is shown in fig. 6.17. It can be observed from the plot that the increase in temperature in the peripheral region (towards the end of line 1 and line 2) is more for z = 9 mm than z = 27 mm.

6.2.3 Freezing front propagation

Ice front propagation with respect to time for various spraying distances is shown in figs. 6.18, 6.19 and 6.20. Blue color in the images represents the dimension of the ice ball. It can be observed from the images that the ice ball transforms from hemispherical shape to semi-elliptical shape as the time proceeds for all the cases. Breitbart [23] studied the behavior of ice front propagation with respect to time for open spray technique on the living pig skin. He concluded that the ice ball transforms from hemispherical to triangular shape as the duration of spray increases. Similar trend is observed in the simulation results as well. It is interesting to note that the expansion of ice ball is more in radial direction than in the axial direction for all the spraying distances considered in the study. Moreover, the difference in radial and axial dimensions of ice ball increases with respect to time. After 20 s of spray the difference in radial and axial dimensions of ice is found to be 3.4 mm whereas after 60 s it is found to be 7 mm for spraying distance z = 18 mm. During the initial phases of spray, the temperature difference between the tissue surface and cryogen is higher which causes partially hemispherical ice ball formation. As the time proceeds, this temperature difference reduces and already formed ice ball provides harder bed to cryogen droplets to disperse in the radial direction. It causes more spread of ice ball in the radial direction as compared to that in the axial direction. Similar trend in axial and radial dimensions of ice ball is observed for the other spraying distances as well.

6.3 Conclusion

Following conclusions can be drawn from the present study:

- Numerical results are in good agreement with the experimental model.
- Necrotic zone is not inversely propotional to the spraying distance; spraying distance of 18 mm provides the most optimised result in terms of cryoablation.

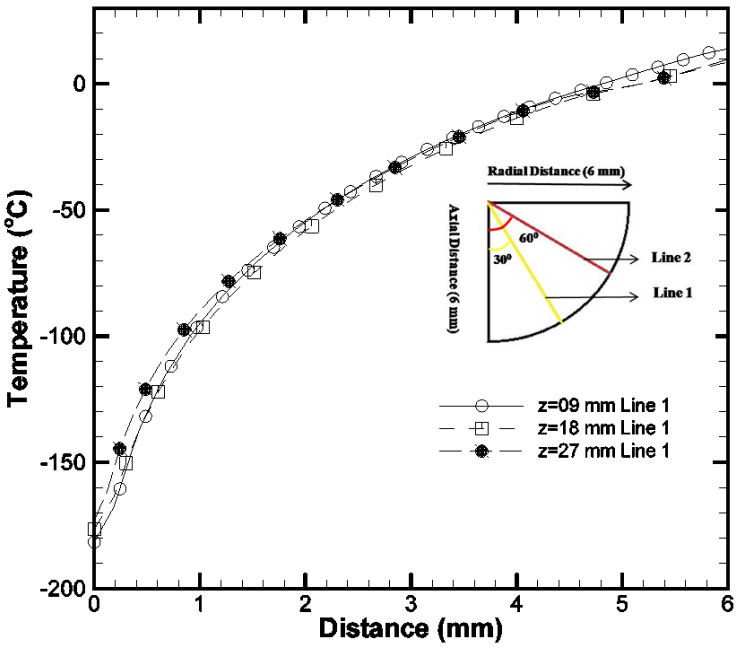

(a) Temperature variation on the line at an angle of 30^0 from spray axis

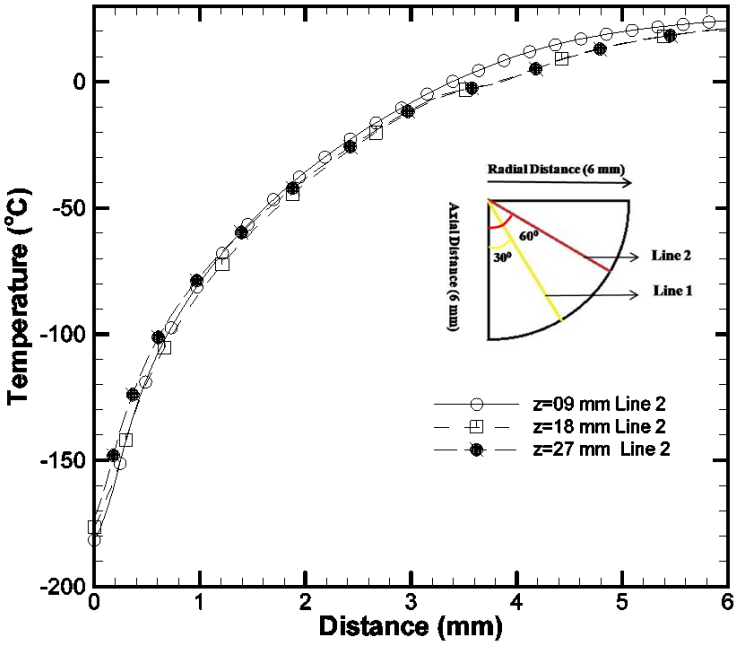

(b) Temperature variation on the line at an angle of 60^0 from spray axis

Figure 6.17: Transient temperature distribution across the tissue domain

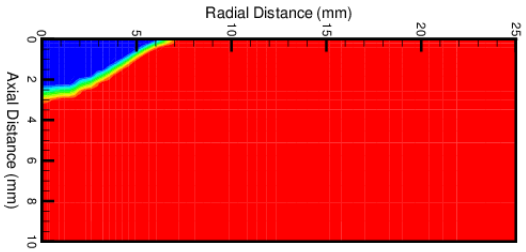

(a) For z = 9 mm

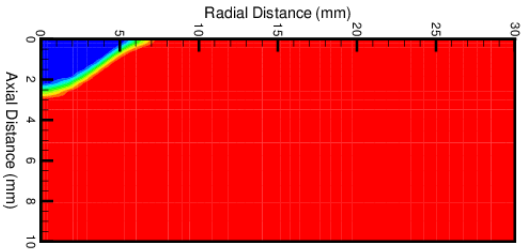

(b) For z = 18 mm

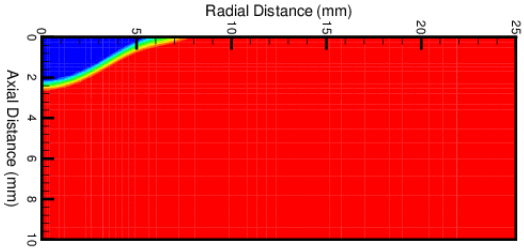

(c) For z = 27 mm

Figure 6.18: Ice front after 20 s

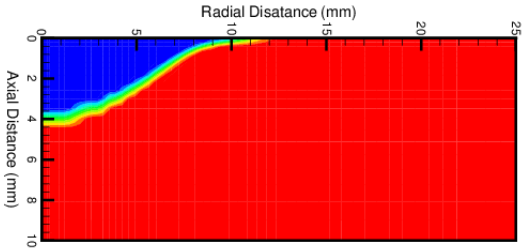

(a) For z = 9 mm

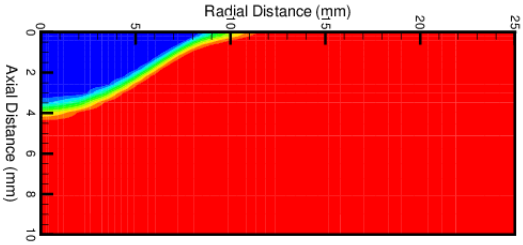

(b) For z = 18 mm

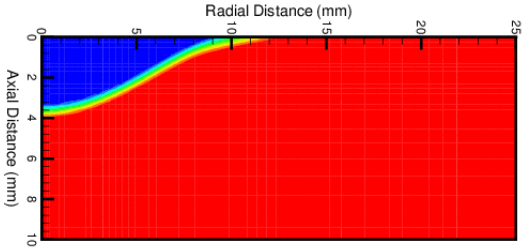

(c) For z = 27 mm

Figure 6.19: Ice front after 40 s

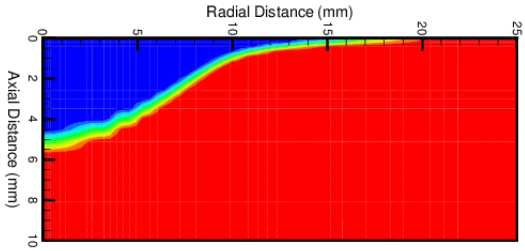

(a) For z = 9 mm

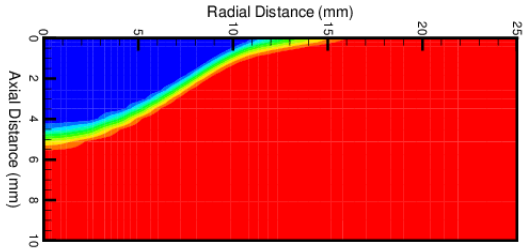

(b) For z = 18 mm

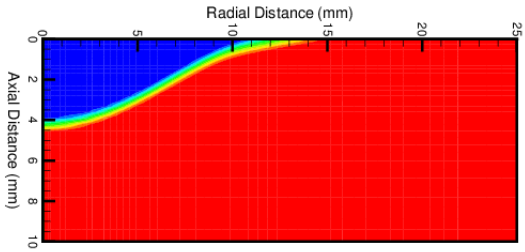

(c) For z = 27 mm

Figure 6.20: Ice front after 60 s

- Cooling capacity of spray in axial direction decreases with increase in the spraying distance whereas it increases in the radial direction.
- Appreciable change in the dimensions of necrotic zone is observed with the change in spraying distance, however drastic change in the dimensions of the halo diameter is observed with the change in spraying distance.
- Even after providing the larger necrotic zone and smaller halo diameter, the spraying distance of 9 mm should not be used while the treatment of lesions occurring near the eye and nose because it causes splashing of the droplets.